

# The large-scale distribution and internal geometry of the fall 2000 Po River flood deposit: Evidence from digital X-radiography

Robert A. Wheatcroft<sup>a,\*</sup>, Andrew W. Stevens<sup>a,1</sup>,  
Louise M. Hunt<sup>a,2</sup>, Timothy G. Milligan<sup>b</sup>

<sup>a</sup>College of Oceanic & Atmospheric Sciences, Oregon State University, Corvallis, OR 97331, USA

<sup>b</sup>Fisheries and Oceans Canada, Bedford Institute of Oceanography, PO Box 1006, Dartmouth, NS, Canada B2Y 4A2

Received 21 October 2004; received in revised form 21 December 2005; accepted 3 January 2006

Available online 20 February 2006

## Abstract

Event-response coring on the Po River prodelta (northern Adriatic Sea) coupled with shipboard digital X-radiography, resistivity profiling, and grain-size analyses permitted documentation of the initial distribution and physical properties of the October 2000 flood deposit. The digital X-radiography system comprises a constant-potential X-ray source and an amorphous silicon imager with an active area of  $29 \times 42$  cm and 12-bit depth resolution. Objective image segmentation algorithms based on bulk density (brightness), layer contacts (edge detection) and small-scale texture (fabric) were used to identify the flood deposit. Results indicate that the deposit formed in water depths of 6–29 m immediately adjacent to the three main distributary mouths of the Po (Pila, Tolle and Gnocca/Goro). Maximal thickness was 36 cm at a 20-m site off the main mouth (Pila), but many other sites had thicknesses  $>20$  cm. The Po flood deposit has a complex internal stratigraphy, with multiple layers, a diverse suite of physical sedimentary structures (e.g., laminations, ripple cross bedding, lenticular bedding, soft-sediment deformation structures), and dramatic changes in grain size that imply rapid deposition and fluctuations in energy during emplacement. Based on the flood deposit volume and well-constrained measurements of deposit bulk density the mass of the flood deposit was estimated to be  $16 \times 10^9$  kg, which is about two-thirds of the estimated suspended sediment load delivered by the river during the event. The locus of deposition, overall thickness, and stratigraphic complexity of the flood deposit can best be explained by the relatively long sediment throughput times of the Po River, whereby sediment is delivered to the ocean during a range of conditions (i.e., the storm responsible for the precipitation is long gone), the majority of which are reflective of the fair-weather condition. Sediment is therefore deposited proximal to the river mouths, where it can form thick, but stratigraphically complex deposits. In contrast, floods of small rivers such as the Eel (northern California) are coupled to storm conditions, which lead to high levels of sediment dispersion.

© 2006 Elsevier Ltd. All rights reserved.

**Keywords:** Po river; Adriatic Sea; Sedimentation; X-radiography; Floods

\*Corresponding author. Tel.: +1 541 737 3891.

E-mail address: raw@coas.oregonstate.edu (R.A. Wheatcroft).

<sup>1</sup>Currently at: US Geological Survey, Menlo Park, CA 94301, USA.

<sup>2</sup>Currently at: Department of Conservation, Southern Islands, PO Box 743, Invercargill, New Zealand.

## 1. Introduction

Small- to moderate-sized rivers ( $10^2$ – $10^5$  km<sup>2</sup>) are especially relevant to sediment dynamics and the development of stratigraphic sequences in the coastal ocean for two reasons. First, despite the fact that most continental interiors are drained by large rivers, such as the Amazon or Mississippi (Vörösmarty et al., 2000), the number of small- to moderate-sized rivers immediately adjacent to the coast is orders of magnitude greater. Thus, sediment discharge by these rivers locally impacts most of the coastal ocean, while the influence of large rivers is restricted to certain areas. For example, along the US West Coast the Columbia River's basin area exceeds that of all other rivers combined, yet its sediment impact is limited mainly to a 100-km long stretch of the Washington margin (Nittrouer et al., 1979; Sternberg, 1986). The influence of small- to moderate-sized rivers may only extend for tens of kilometers from their mouth (Warrick and Fong, 2003), yet that is roughly their spacing along the coast. The second important feature of small rivers is their high sediment yield (i.e., kg/km<sup>2</sup>/y) compared to large rivers. Due to a variety of factors, for example, greater tectonism, steeper channel gradients and decreased storage capacity in the basin, small-river yields may be higher by 2–3 orders of magnitude (Milliman and Syvitski, 1992; Hicks et al., 2000). Thus, these rivers may be inconsequential for freshwater and solute inputs to the global ocean, but they cannot be neglected from the standpoint of sediment delivery and accumulation (Milliman and Syvitski, 1992; Mulder and Syvitski, 1995).

The discharge of small rivers also fluctuates more than large systems. For example, peak discharge of many rivers on the US West Coast or the Mediterranean may be up to 40 times greater than base level, whereas the discharge of large rivers may increase by only a factor of two during floods (e.g., Gomez et al., 1995). Because suspended-sediment concentration and hence sediment load is a positive, non-linear function of fluid discharge, the tendency for small rivers to flood has important implications for the timing and mechanics of sediment delivery to the coastal ocean. It is likely that the majority of sediment flux from small rivers occurs during short-lived (day to weeks) events (e.g., Wheatcroft et al., 1997; Inman and Jenkins, 1999; Restrepo and Kjerfve, 2000), thereby underscoring the key relevance of floods to coastal sedimentation. The

challenge of studying flood sedimentation is that although many rivers flood each year, it is impossible to predict when a particular river will flood. Therefore, an event-response sampling approach is necessary (Wheatcroft, 2000), yet due to ship scheduling practices and an expeditionary mindset of oceanographers whereby cruises are planned months to years in advance, this has been rare in the past (see, however, Drake et al., 1972; Pelletier et al., 1999).

Event-response sampling played a key role in elucidating the large-scale distribution, small-scale physical and chemical properties, and formative mechanisms of several flood deposits on the continental shelf offshore northern California's Eel River (Wheatcroft et al., 1997; Drake, 1999; Leithold and Hope, 1999; Sommerfield et al., 1999; Wheatcroft and Borgeld, 2000; Geyer et al., 2000; Hill et al., 2000; Traykovski et al., 2000). Relevant characteristics of the Eel flood deposits are as follows. First, the depocenter of the flood deposits was located roughly 18 km from the river mouth at a water depth of 70 m (Wheatcroft et al., 1997; Wheatcroft and Borgeld, 2000). Second, the flood deposits extended for about 30 km in the along isobath direction, but only 8 km in the across isobath direction, residing in water depths of 50–110 m. Third, the maximal thickness of the Eel flood deposits was 8 cm, thus horizontal thickness gradients were small. Lastly, the flood deposit was stratigraphically simple, i.e., a single bed. Because oceanic floods are rare and observations of flood deposits on continental shelves are even rarer, it is uncertain to what extent the characteristics of the Eel flood deposits might apply to oceanic flood deposits formed by other rivers; additional realizations were sorely needed.

Soon after the termination of the Eel River studies, an opportunity arose to respond to a major flood of the Po River, which discharges into the northern Adriatic Sea. The flood in question occurred during October/November 2000, and event response sampling in early December of that year and during several cruises over the succeeding 2.5 years has provided detailed knowledge regarding the initial character of the flood deposit and its subsequent biological and physical alteration. The latter subject is treated in a separate communication. Our primary objective herein is to describe the initial large-scale distribution and internal properties of the Po 2000 flood deposit. In addition, we will compare and contrast the Po flood deposit with

the Eel River flood deposits. These two rivers provide some important contrasts and similarities. For example, the Po has multiple distributary mouths, while the Eel does not. Both discharge onto open continental margins, yet characteristics of their receiving basins (e.g., coastal circulation, wave climate) differ. Therefore, potential contrasts in their flood deposits may have predictive value—if the controlling variables can be identified. An additional goal of this paper is to describe in detail a new digital X-radiography system that was used in studying the Po flood deposit. X-radiography is of course not a new tool in sedimentary geology (Hamblin, 1962; Howard, 1968; Krinitzsky, 1970), but recent technical advances have provided new opportunities (e.g., Migeon et al., 1999), especially post-acquisition processing of the data. Thus, we will describe and apply several image processing algorithms that were used to objectively identify the Po flood deposit.

## 2. Study site and methods

### 2.1. The Po River system

The Po River, the largest river in Italy (basin size of  $\sim 7 \times 10^4 \text{ km}^2$ ), has important implications for freshwater, solute, and particulate balances in the Adriatic Sea. The river heads in the Pennine and Maritime Alps (maximal relief  $> 4000 \text{ m}$ ) to the north and west and the Apennine Mountains ( $> 2400 \text{ m}$ ) to the south, and then flows over a wide, low-gradient alluvial plain, where a significant fraction of Italian agricultural and industrial output occurs. Average annual discharge is  $\sim 1500 \text{ m}^3/\text{s}$  (Nelson, 1970), with climatological peaks in late spring due to snowmelt and in late fall from intense precipitation events. Since the instrumental record began in 1918 there had been five floods with discharges  $> 8500 \text{ m}^3/\text{s}$  (measured at the Pontelagoscuro gauging station, 120 km upstream from the mouth) with the most recent in fall of 1994. Historical evidence of course indicates many other large events during the past two millennia (e.g., Pavese et al., 1992).

Before reaching the Adriatic Sea the main stem of the Po River forms four major distributary channels within the delta; from north to south, these are the Pila, Tolle, Gnocca (or Donzella) and Goro (Fig. 1). Of these four, the Pila carries the majority of water and sediment ( $\sim 70\%$ ), with secondary contribu-

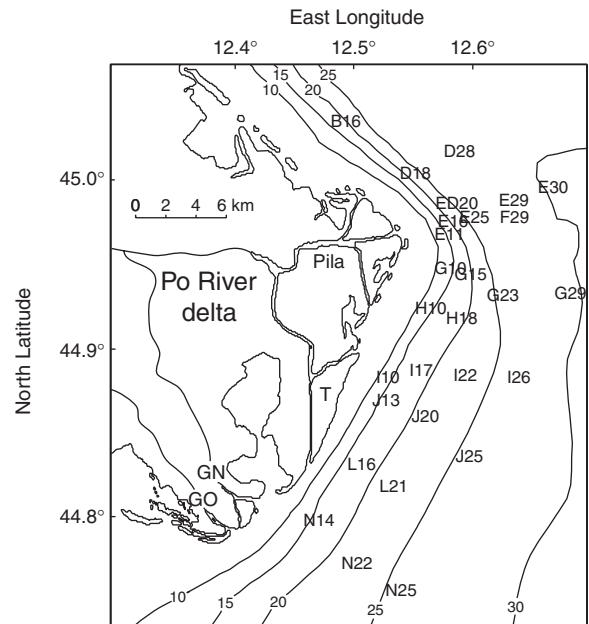


Fig. 1. Map of the Po River delta and adjacent prodelta showing the location and numbering scheme of stations, as well as the general bathymetry (in meters) and river mouth locations (Pila, T = Tolle, GN = Gnocca, GO = Goro). Stations are identified by letters that refer to roughly shore-normal transects and nominal water depths (e.g., E29 is on the E line at roughly 29 m).

tions from the Gnocca (11%), Goro (8%) and Tolle (7%) (Nelson, 1970; Syvitski et al., 2005). Upon entering the ocean sand is deposited adjacent to the river on the delta front (Boldrin et al., 1988), while offshore ( $> 5\text{--}10 \text{ m}$ ) there is a well-developed prodelta mud wedge that extends to a water depth of roughly 30 m, where the mud intergrades with a relict sand unit (e.g., Trincardi et al. 1994). The bathymetric slope is fairly steep in the northern portion of the prodelta (Fig. 1), but moderates considerably to the south (off the Tolle and Gnocca/Goro). Sediment accumulation rates in the immediate vicinity of the Po based on  $^{210}\text{Pb}$ -geochronology range from 0.2 to  $> 1 \text{ cm/year}$  (Frignani et al., 2005).

### 2.2. The Fall 2000 flood

Beginning in early October 2000, several periods of intense rainfall primarily in the northwestern portion of the Po basin (Valle d'Aosta) resulted in substantial landslides and flooding (e.g., Ratto et al., 2003). The resultant peak discharge ( $9650 \text{ m}^3/\text{s}$ ) measured at Pontelagoscuro on October 20 had

been exceeded only twice since 1918. During the full extent of the event (1 October to 31 December 2000) the Po River discharged roughly  $34 \times 10^9 \text{ m}^3$  of water, which is 71% of the long-term annual average. The flood hydrograph displayed three (10/20, 11/9 and 11/20) daily discharge peaks that exceeded  $6000 \text{ m}^3/\text{s}$  (Fig. 2).

In response to the late October event, investigators at the Istituto di Scienze Marine (CNR-Bologna), the University of Washington and Oregon State University conducted an event-response cruise in early December 2000. By definition there was little time to plan this cruise, and only a modest effort could be mounted. Activities mainly focused on determining, via seabed coring, the presence and distribution of a flood deposit, although some water column sampling was also conducted. A series of 4-day cruises were conducted out of the port of Marina di Ravenna on board the M/V Sarom VIII, a  $\sim 27\text{-m}$  gas-field support vessel. Seabed samples were acquired with a  $20 \times 30 \text{ cm}$  Ocean Instruments box corer. From the box cores a variety of subcores were collected for subsequent shipboard and laboratory analyses (e.g., resistivity, radionuclides, organic carbon). A total of 33 stations were occupied in water depths from 10 to 30 m adjacent to the Po delta (Fig. 1). Following results obtained during studies of the Eel River flood deposits (e.g., Wheatcroft et al., 1997; Wheatcroft and Borgeld, 2000), the primary means to identify presence/absence of a flood deposit was X-radiography of subcores, although radionuclides ( $^7\text{Be}$ ,  $^{234}\text{Th}$ ) proved useful as well (Palinkas et al., 2005). New to this effort, however, was a fully digital X-radiography system.

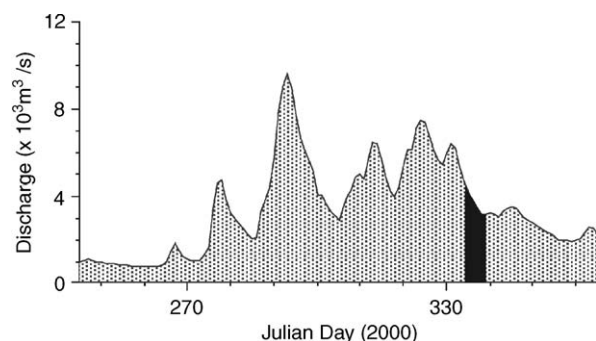


Fig. 2. Daily average discharge measured in thousands of  $\text{m}^3/\text{s}$  at Pontelagoscuro ( $\sim 120 \text{ km}$  from the river mouth). The black region denotes the December 2000 sampling cruise. Discharge source: Regione Emilia-Romagna (2001).

### 2.3. Digital X-radiographic system

There are two main elements of the digital X-radiography system used herein: an X-ray source and a detector (Fig. 3). The X-ray source is a Lorad LPX-160 industrial X-ray generator that comprises a tube head, a liquid cooling unit and a control unit (the latter two components are not shown in Fig. 3). The tube head is an end grounded, exposed anode configuration with a thin beryllium window, and is capable of producing X-ray energies up to 160 kV at 1-kV increments with a maximal tube current of 5 mA adjustable at 0.1-mA increments. An important characteristic of the X-ray source is that the voltage and tube current during an exposure are stable to within  $\pm 1\%$ , thus the cumulative X-ray flux of sequential exposures is approximately steady. This stability is demonstrated by the extremely small between-radiograph variability in brightness of a calibration module ( $\sim 1\%$  coefficient of variation; Sokal and Rohlf, 1981).

The most important component of the system is the X-ray detector: a dpiX Flashscan 30 imager (Fig. 3). This device is a high-resolution amorphous silicon (a-Si) detector that utilizes a Kodak Lanex Fine<sup>®</sup> phosphor screen coupled to an array of a-Si photodiodes that detect visible light and thin-film transistors that connect the photodiodes to the readout electronics (Weisfield et al., 1998). Salient characteristics of the imager are a  $29.3 \text{ cm} \times 40.6 \text{ cm}$  (width  $\times$  height) active area, a pixel spot size of

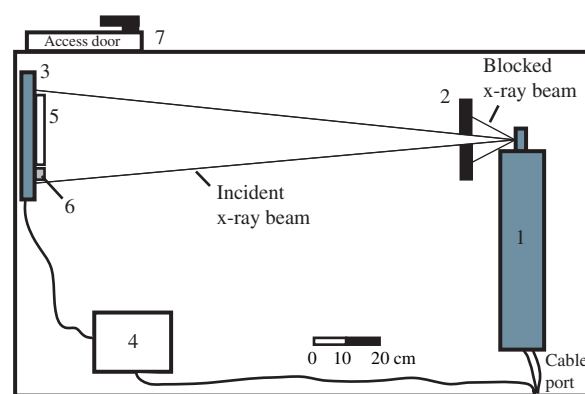


Fig. 3. Schematic plan view of the digital X-radiography system. 1 = Tube head (Lorad LPX-160), 2 = lead shielding that blocks a portion of the X-ray beam, 3 = digital imager (dpiX Flashscan 30), 4 = power supply for imager, 5 = sample container, 6 = calibration module (see text), 7 = lead-lined cabinet with access door. Electronics cables lead to the computer workstation, tube-head cooler and X-ray control unit.

127  $\mu\text{m}$  resulting in an image size of  $2304 \times 3200$  pixels, and a 12-bit depth resolution (i.e., 4096 gray levels). The resultant digital X-radiographs are indistinguishable from those collected using film, yet they are acquired in near real time and are immediately available for post-acquisition image processing.

Ancillary equipment associated with the system includes a computer running Windows NT, a 14-mm thick lead sheet that limits the X-ray beam to the imager's active area and a lead-lined cabinet with safety interlocks that houses the tube head and the detector (Fig. 3). Both the X-ray source and the detector are controlled remotely, thereby facilitating shipboard use of the system. A typical imaging sequence consists of exposing the detector at 70 kV and 5 mA for a total of 28 s. During the first  $\sim 5$  s of the exposure the tube head is ramping up to the full voltage and tube current output, at +6 s the imager is actuated, which leads to a 6.4-s long period during which charges are accumulated. To minimize electronic noise, three successive scans are stored temporarily and the average brightness of each pixel sent through a shielded RS-485 to the computer. To calibrate radiographs for bulk density determination, a 36-cm tall  $\times$  4-cm wide calibration module consisting of 16 ( $2 \times 4.5$  cm) sections of varying thicknesses of glass that correspond to bulk densities between 1 and  $2.07 \text{ g/m}^3$  is present within each image (discussed below).

#### 2.4. Radiograph segmentation techniques

Digital images can be manipulated in both the spatial and frequency domain using a wide range of algorithms that correct, enhance, segment, extract and classify information contained within them (e.g., Gonzalez and Wintz, 1987; Jähne, 1991; Russ, 1995). Herein, our primary focus is on *image segmentation*, whereby an image is subdivided into regions that correspond to distinct units within the scene (Wilson and Spann, 1988). In particular, we are interested in using algorithms that objectively separate flood sediment from ambient, pre-flood sediment. The first step in achieving this goal is to consider which characteristics of a flood deposit that are sensible by X-radiography can be used to distinguish flood sediment from ambient sediment. Based on our conceptualization of flood sedimentation and supported by results from the Eel margin (e.g., Wheatcroft and Borgeld, 2000), at least three

characteristics of flood deposits may be exploited using digital X-radiography.

First, flood sediment typically has a much higher porosity (lower bulk density) compared to ambient sediment (Wheatcroft and Borgeld, 2000). High porosity may be due in part to the elevated clay content of flood sediments (e.g., Hill et al., 2000; Wheatcroft and Borgeld, 2000; Milligan et al., 2006), but also to the fact that rapid deposition leads to under-consolidated beds (e.g., Meade, 1966). Because X-ray attenuation and therefore the brightness of an X-radiograph depends in part upon the bulk density of the object, relative brightness changes may be used to segment flood sediment from ambient sediment. Using pixel brightness to segment an image is called *thresholding* (Russ, 1995), and requires creation of a brightness histogram (counts of pixel brightness over the entire image). Ideally the brightness histogram is bimodal and the pixel value at the trough clearly segments the scene resulting in a binary image (Fig. 4A and B).

Second, by definition a discrete sedimentary layer such as a flood deposit must have a contact with the underlying sediment, otherwise it would be indistinguishable from that unit. Thus, if a flood deposit differs from ambient sediment due, for example, to grain size, bulk density or fabric, then its lower contact should be identifiable using an edge detection algorithm. We explored a variety of one- and two-dimensional edge detection algorithms based on first and second derivatives in brightness (e.g., Sobel, Roberts and Laplace operators, Jähne, 1991; Russ, 1995), but found them to be particularly sensitive to small-scale brightness variations. Therefore we developed a two-step algorithm that yielded an "edge map". The first step, removal of vertical edges caused by shell debris or biogenic structures, involved application of a 20 pixel (horizontal) median filter (Jähne, 1991) to the image. Next, based on pretests of a subset of images that showed contacts occurred over roughly 2 mm, we applied a 15-pixel (vertical) mask that calculated the maximal range within that domain. The resultant edge map contained high values where horizontal contacts existed (Fig. 4C).

The third diagnostic characteristic of flood beds that can be quantified using digital X-radiographs is lack of biogenic sedimentary structures. In most settings, benthic infauna bioturbate the upper 10–20 cm of the seabed and produce a complex sedimentary fabric comprising tubes, burrows and

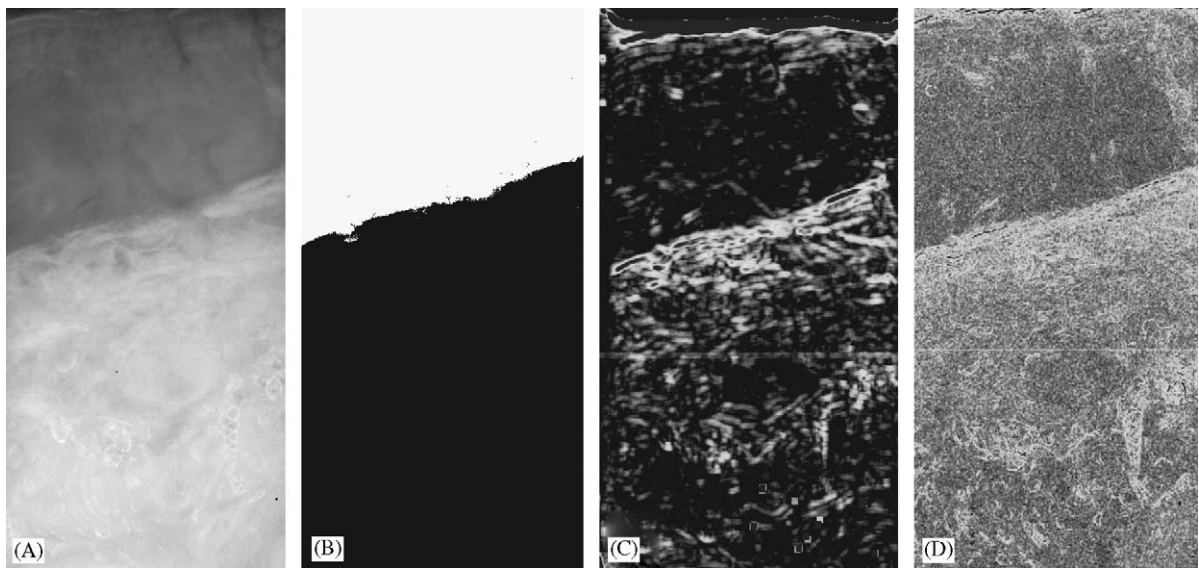


Fig. 4. X-ray negative (A) and the results of a brightness threshold (B), the horizontal edge detection algorithm (C) and the texture algorithm (D). Bright pixels in (C) and (D) indicate horizontal edges (i.e., contacts) and large variations in local brightness (i.e., bioturbated sediment), respectively (see text for details).

various feeding structures. This “ichnofabric” or bioturbate texture (Frey and Pemberton, 1990) is readily sensed in X-radiographs because the small-scale packing heterogeneities lead to variability in attenuation (hence brightness). Newly deposited sediment layers, such as flood beds, generally lack well-developed biogenic structures because infauna have been killed or displaced vertically (i.e., animals have re-established their living positions adjacent to the sediment–water interface). That is not to say that biogenic structures are always absent in flood layers, as recolonization by benthic fauna can occur rapidly (e.g., Pelletier et al., 1999; Wheatcroft, 2006), but simply that freshly deposited sediment has a less well-developed bioturbate structure than older deposits. To quantify bioturbate texture we calculated the standard deviation of brightness in a  $20 \times 20$ -pixel mask (2.5 mm on a side). Areas of high brightness variability were associated with the buried sediment water interface, whereas the flood deposit generally had much lower brightness variability (Fig. 4D). Significant noise associated with this measurement precluded its use in segmentation, but it was helpful in interpreting results based on bulk density and contacts.

### 2.5. Absolute bulk density

High-resolution measurements of absolute bulk density were used to provide an estimate of the total

mass of sediment in the flood deposit, as well as information on the internal properties of the deposit. Extracting accurate bulk density data from the digital X-radiographs required several steps. First, a vertical beam correction algorithm was applied to the raw images that removed brightness variations observed in a target of uniform thickness and composition (Plexiglas bar) present in each radiograph. Although horizontal variations in the X-ray beam intensity were also noted, these were generally much smaller than vertical variations and were negligible over the horizontal domain examined in subsequent steps. Second, a relationship (Fig. 5A) was established between brightness averaged over a 5-mm vertical  $\times$  50-mm horizontal mask and the bulk density measured using a shipboard resistivity profiler (e.g., Andrews and Bennett, 1981; Wheatcroft and Borgeld, 2000; Wheatcroft, 2002). The resistivity profiles, which were collected from the same box core, but not the X-ray slabs themselves, were bin averaged over the same vertical domain. The horizontal extent of the resistivity probe is on the order of 3 mm. Third, a second-order polynomial was used to relate pixel brightness to bulk density for the entire X-radiographs, from which vertical profiles of bulk density were extracted (Fig. 5B). Note that a calibration using gravimetrically determined water content data is required to relate the resistivity data to bulk density, and this step results in an uncertainty of

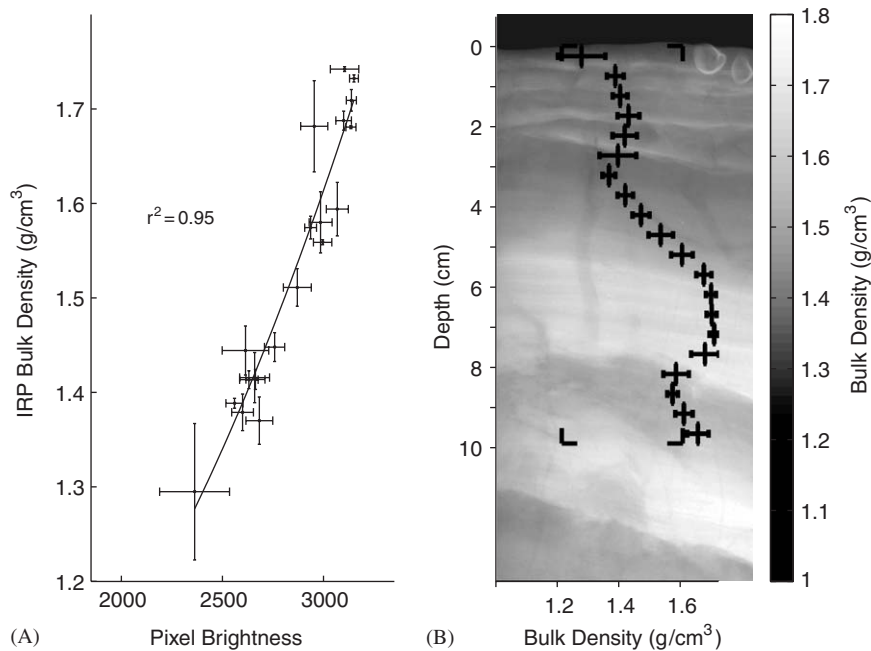


Fig. 5. Representative example illustrating steps converting X-radiograph brightness to bulk density. (A) A regression equation (not shown) from a plot of pixel brightness versus bulk density determined from a shipboard resistivity profiler (e.g., Wheatcroft, 2002) is used to relate pixel brightness to bulk density (B). The vertical profile of bulk density in (B) represents a 5 mm × 50 mm (height × width) average ( $\pm$  standard deviation).

$\pm 5$ –10% (Andrews and Bennett, 1981; Wheatcroft, 2002). The overall uncertainty associated with bulk density estimates based on the digital X-radiographs is therefore in the range of 10–15%.

## 2.6. Sediment texture

The disaggregated inorganic grain size (DIGS) was determined for subsamples from each core following the methods described in Milligan and Kranck (1991). Briefly, samples were collected from the X-ray slabs using the digital X-radiographs as guides. In the laboratory, samples were dried at  $<60^\circ\text{C}$ , digested in 35% hydrogen peroxide and then resuspended in a 1% NaCl solution. Immediately prior to analysis on a Coulter Multisizer IIe, sediment was disaggregated using a sapphire-tipped ultrasonic probe. Results are expressed as equivalent weight percent calculated from the volume analyzed using a specific gravity of  $2.65\text{ g/cm}^3$ , and plotted as log equivalent weight (%) vs. log diameter to preserve the shapes of the distributions over a wide range of concentrations (Kranck and Milligan, 1991).

## 3. Results

### 3.1. Large-scale distribution

X-radiographs of cores collected in December 2000 contained unequivocal evidence of newly deposited sediment. Diagnostic features observed within the X-radiographs as well as the cores themselves included: (1) thick (several centimeter), parallel beds with abundant physical sedimentary structures (e.g., cross bedding, laminations, soft sediment deformation structures) and sharp upper and lower contacts, (2) scattered biogenic structures, but little evidence of intense bioturbation of the sort that was observed in subsequent sampling cruises, and (3) extremely low bulk densities. All of these features permitted the ready application of the segmentation algorithms described above.

The bulk density segmentation method based on brightness thresholding identified a flood deposit at 17 of the 33 stations. Maximal thickness observed using this technique was 23 cm at station J13 (off the Tolle), and minimal (but non-zero) thickness was 1 cm at station I17 (cf. Fig. 1). Stations where the bulk density method did not identify a flood layer

were of two types. First, at 12 stations the brightness histogram within the sediment was unimodal (i.e., there was no contrast in brightness). These stations were mainly in the deeper ( $>20$  m) portions of the study area and distal to the main mouth where there was no evidence of a flood bed (in this sense the brightness segmentation algorithm “worked”, as it did not falsely identify a flood bed). At four other stations, mainly proximal to the Pila mouth, presence of an X-ray opaque layer (e.g., Fig. 6) within the deposit precluded straightforward use of the bulk density method.

In general, the edge detection algorithm provided similar results to the bulk density method. Maximal thickness observed in the box cores was 26 cm at station E11, directly off the Pila, and minimal thickness (1 cm) was observed at several sites (e.g., B16, I17) within the study region (cf. Fig. 1). Again, the edge detection algorithm did not detect a flood layer at several offshore, distal sites—consistent with the results from the bulk density method. At

nine stations within the study region, generally proximal to the river mouths (e.g., E11, G10, H10, N14), the edge detection algorithm identified multiple contacts within the overall flood deposit. In these cases, the flood deposit thickness was based on the deepest contact observed within the box core (see below for a discussion that supports this action). At two stations, D18 and J25, the edge detection algorithm either did not identify the deepest contact present (D18) or misidentified a large biogenic structure in the subsurface as a contact (J25). In the former case, a thin, X-ray opaque layer (the “coarse-silt layer” discussed below), at  $\sim 12$  cm below the sediment–water interface yielded a readily identified contact, however, another 8 cm of fresh unbioturbated sediment clearly existed below this contact. We therefore assigned a flood layer thickness of 20 cm at this station—consistent with adjacent stations.

The texture algorithm typically yielded noisy results that precluded objective segmentation. The

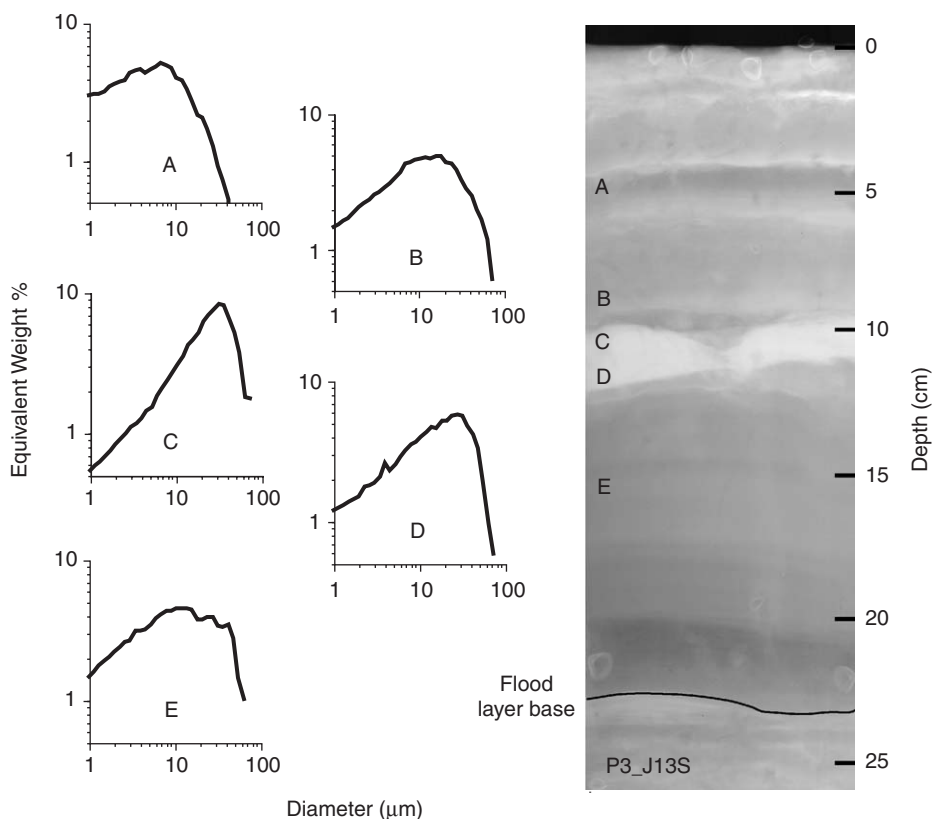


Fig. 6. X-radiograph from station J13 (June 2001) showing a roughly 23-cm thick flood deposit with a distinct X-ray opaque layer at 10–11 cm depth. Grain size analyses at the vertical positions designated as A–E indicate that the X-ray opaque layer is composed of relatively well-sorted coarse silt.

main sources of noise within the flood deposit were laminations and scattered shell debris, both of which create large brightness contrasts. Nevertheless, the texture algorithm proved to be useful in interpreting the results of the edge detection algorithm. In particular, at stations where multiple beds, and hence contacts existed within the flood deposit (e.g., E11, G10, H10, N14), the texture algorithm measured approximately uniform brightness variation between beds. In contrast, brightness variation typically increased when crossing the lowermost contact. We interpreted this increase to be associated with the buried, pre-flood sediment that had a well-developed bioturbate texture.

To provide a visual summary of the flood deposit thickness, an isopach map of the fall 2000 flood deposit was created (Fig. 7). Several steps and assumptions were made to create the isopach map. First, the December 2000 data coverage was extended by using thickness data from X-radiographs collected during an October 2001 cruise. To verify the comparability of the latter data, flood deposit thickness at several stations determined independently in December 2000 and October 2001 was compared and found to agree within  $\pm 2$ –3 cm (similar to within-station variability). Second, X-radiographs taken along the shallow portion of the E line (E11–E20) indicated that the box cores

taken in December 2000 did not penetrate the flood deposit (i.e., bedded, unbioturbated sediment was observed to the base of the core). X-radiographs of a kasten core collected at E20 in April 2002 indicated the base of the flood deposit was at  $\sim 36$  cm. We therefore, assigned a similar thickness to E11 and E16 where there were similar bedding sequences in the X-radiographs. Third, the inner (landward) boundary of the flood deposit was set at 5-m water depth. This action was based on results from grab sampling (June 2001) and box coring (June 2003) that showed thick, muddy beds at depths of 6–8 m, but only sand at 5 m (T. G. Milligan, unpublished results). Fourth, the offshore extent of the flood bed was limited by inserting dummy stations with zero thickness values between stations where no flood deposit was detected. Failure to take this step resulted in a tendency for the contouring algorithm to spread the deposit offshore. Lastly, the contouring algorithm was based on a Delaunay triangulation with linear interpolation (Davis, 1986).

The isopach map shows clearly that the flood deposit was found in shallow water (10–25 m), and formed three depocenters associated with the Pila, Tolle and Gnocca/Goro distributary mouths (Fig. 7). Offshore of the former, the flood deposit is fairly thick ( $\sim 20$  cm) in water depths  $> 20$  m, whereas off the Tolle and Gnocca/Goro mouths, the flood deposit thins to  $< 10$  cm in water depths of 15–20 m (Fig. 8). In the northern portion of the prodelta the flood deposit extends to 29 m, whereas in the south it extends to  $\sim 25$  m (Tolle) and  $\sim 20$  m (Gnocca/Goro). Therefore, it would appear that there is a lateral thinning of the deposit to the south. In general, thickness gradients are anisotropic with larger gradients in the cross-isobath direction, but even in the along-isobath direction the thickness gradients can be large.

### 3.2. Small-scale bedding and physical properties

The Po River flood deposit exhibits a remarkably diverse array of stratal types and physical sedimentary structures (Figs. 9 and 10). Layer thickness within the flood deposit ranged from sub-millimeter, parallel laminae (Fig. 9C) to almost structureless beds  $> 10$  cm thick (Fig. 9D). Examples of cross-lamination (Fig. 9E) and lenticular bedding (Fig. 9A and C) were associated with a coarse silt bed (Fig. 6C and D) observed at many shallow-water (10–15 m) stations, especially near the mouths of the

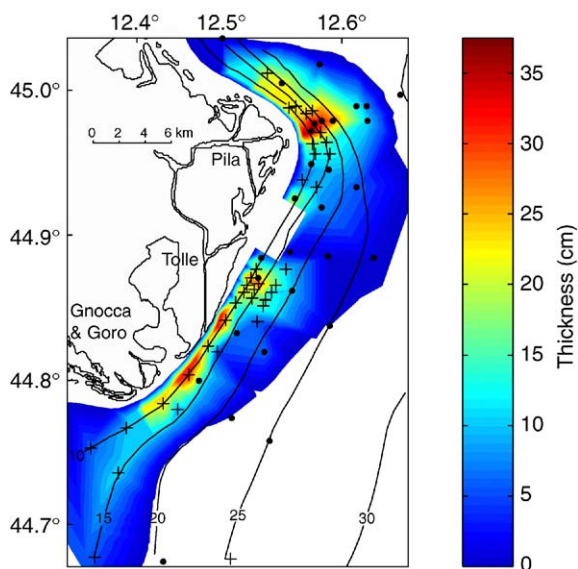


Fig. 7. Isopach map of the fall 2000 Po River flood deposit based on sampling in December 2000 (•) and October 2001 (+). The rectangular area between the Pila and Tolle that lack data is a large mussel farm that precluded sampling. See text for details.

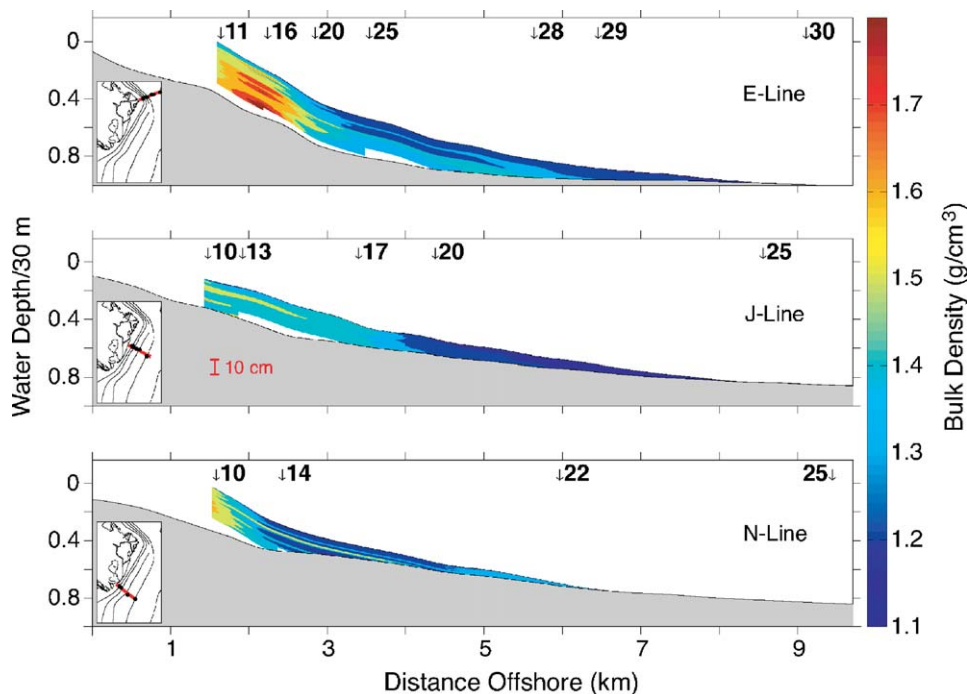


Fig. 8. Cross-margin depictions of the flood deposit thickness and bulk density off the Pila (E line), Tolle (J line) and Gnocca (N line) distributary mouths. Sampling depths (in meters) are denoted at the top of each panel and the y-axis is scaled at 1/30th the water depth (e.g., 0.4 = 12 m).

Tolle and Pila. At several other shallow stations, there are well-developed examples of fining upward beds (Fig. 10). In addition, several examples of soft-sediment deformation structures were observed on the E-line transect offshore the Pila (Fig. 9A and B).

#### 4. Discussion

Three general topics are discussed in the following. First, the efficacy of the digital X-radiography system is examined in general and in relation to objectively identifying the Po River flood deposit. Second, the characteristics of the flood deposit within the context of the Po River dispersal system (i.e., without regard to other river systems) are discussed. Third, the large- and small-scale properties of the Po River flood deposit are compared to results from the Eel River margin (e.g., Wheatcroft et al., 1997; Wheatcroft and Borgeld, 2000).

##### 4.1. Digital X-radiography

Shipboard digital X-radiography as described herein has several advantages over conventional, film-based radiography. First, X-radiographs are

obtained in near real time during the sampling cruises (typically within <0.3 h of coring). Therefore one obtains accurate assessment of, for example, presence or absence of a flood bed, that allows for adaptive sampling and more efficient use of ship time. In addition, the rapid acquisition of the radiographs minimizes post-collection disturbances (i.e., between core and image collection). The importance of the latter cannot be overstated, as there are many physical (e.g., compaction from high-frequency vibrations that are ubiquitous on ships) and biological (e.g., aberrant bioturbation caused by animals undergoing temperature or oxygen stress) processes that quickly alter the sediment fabric in important ways. Thus, the much-touted CT scanning technique (e.g., Orsi et al., 1994), which typically requires prolonged transport of cores to a land-based facility, will continue to yield tenuous results in certain areas of inquiry (e.g., consolidation, biogenic sedimentary structures) until a shipboard system is developed.

A second advantage of digital X-radiography is that the response of the imager to a given exposure is from a practical standpoint more consistent than a system based on film. The latter modality contains

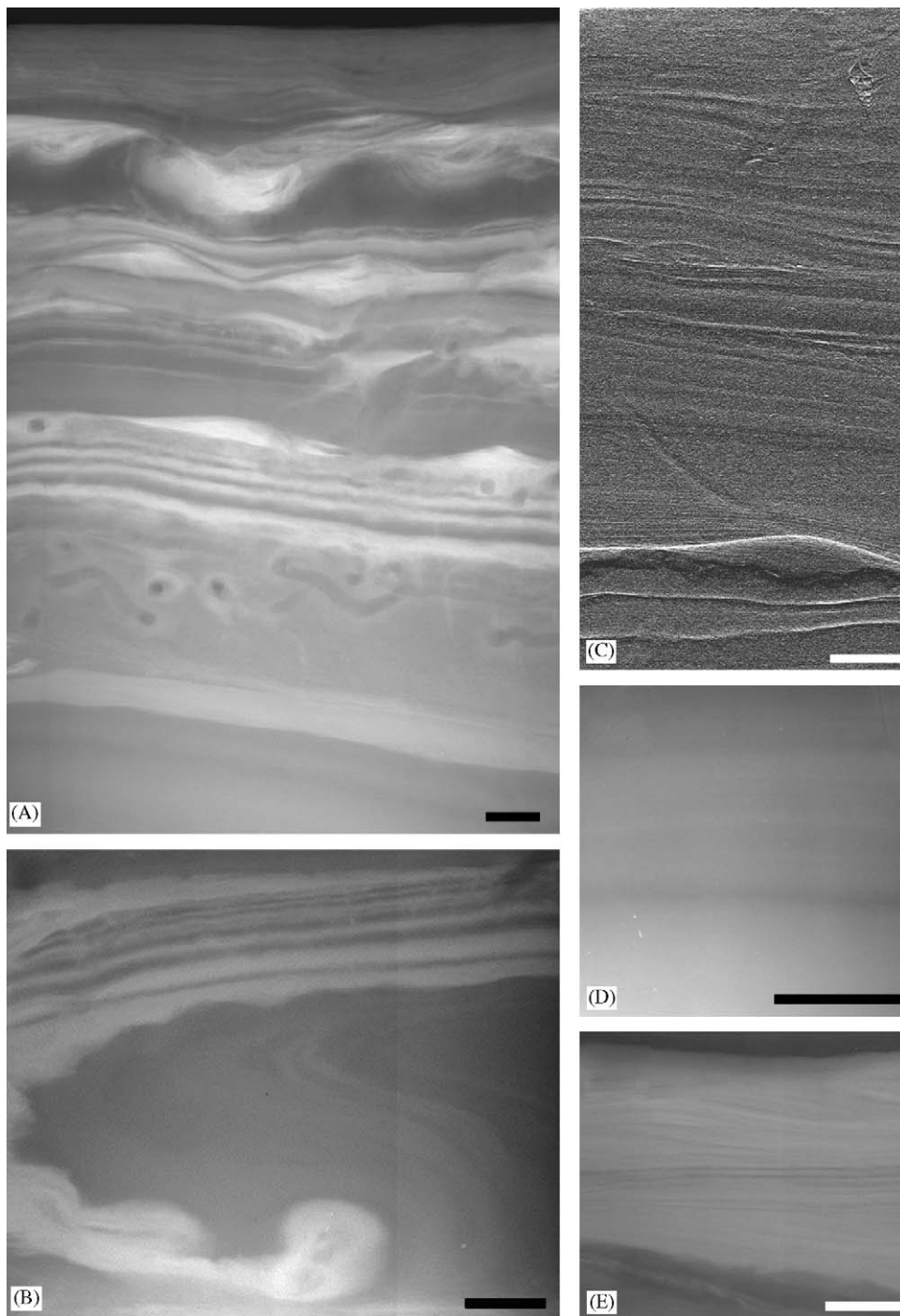


Fig. 9. Representative stratal types and physical sedimentary structures observed in digital X-radiographs along the E line. (A) Soft-sediment deformation structures, lenticular bedding and laminations at E11, (B) soft-sediment deformation structure at E16, (C) enhanced X-radiograph showing lenticular bedding and laminations at E20, (D) diffuse bedding observed in the lower portion (> 20 cm depth) of the flood deposit along the E line (example is from E25), (E) ripple cross-bedding in the coarse-slit layer (cf. Fig. 6) at E20 (June 2001). In all panels the scale bar is 2 cm.

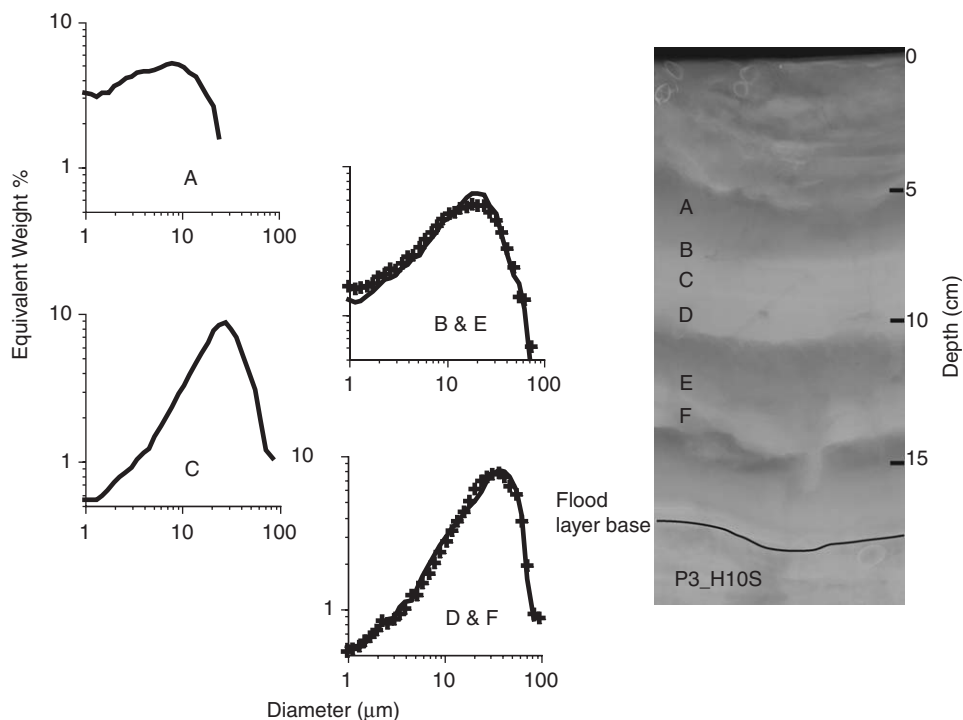


Fig. 10. X-radiograph from station H10 (June 2001) showing an approximately 18-cm thick flood deposit with three beds that become more X-ray opaque upwards. Grain size analyses at positions A–F indicate that the beds fine upward and that the pattern repeats itself vertically (e.g., compare grain size spectra at the base of the beds (D and F). Grain size spectra for E and F are denoted by pluses.

significant room for random variation during the film developing stage due, for example, to variations in temperature and chemical strength, as well as inconsistencies in the film emulsion (Dance, 1988). Although some of this variation can be minimized and corrected, doing so involves specialized developers and densitometers that are rarely used in marine science. Therefore, like CT, digital X-radiography permits the direct extraction of quantitative information such as absolute bulk density. Third, digital images permit the application of post-acquisition processing algorithms for purposes of enhancement and segmentation. Although film X-radiographs can be scanned, scanners capable of capturing the optical depth of X-radiographs are quite expensive, and it is far more efficient if this additional step can be omitted. Lastly, having X-radiographs in digital form allows for wide dissemination of results to colleagues, who can then use the images to guide subsampling. Digital X-radiography is not without some disadvantages, however. For example, the current cost of X-ray imagers is several tens of thousands of US dollars, and they are of uncertain endurance when subject to

the harsh conditions of research vessels. In addition, creating a hard copy of the X-radiograph requires an additional step and hardware, whereas a hard copy is an explicit end result of film-based radiography.

No single image-processing algorithm proved capable of identifying correctly the flood deposit thickness at all sites. Stratigraphically complex deposits that contain X-ray opaque units (e.g., Fig. 6) can compromise the brightness (bulk density) segmentation algorithm. In addition, if the ambient (pre-flood) sediment has a high porosity, then the brightness thresholding may not correctly identify a flood deposit. Thus, flood beds emplaced distally from a river mouth may be more difficult to identify, because distal sediments are apt to have a higher porosity (note that this is not the case on the Po margin where offshore sediments are relict, coarse-grained sediments with low porosity). The edge detection (contact) algorithm proved to be more robust compared to the brightness threshold method in the sense that it provided a result at a larger number of stations, but it did yield several “false positives” (i.e., cases where the algorithm

identified a contact, but other information suggested that contact was not the base of the flood deposit). Again, false positives mostly occurred at sites with a complex deposit where multiple contacts existed (e.g., Fig. 9A). In addition, large, horizontally oriented biogenic structures can mimic a bed contact. Fortunately, such structures are not common and they do not extend over appreciable horizontal distances, thus they can be readily identified by viewing multiple radiographs taken from the same box core. Although the last algorithm, texture mapping, was too noisy to be objectively segmented, it did prove to be invaluable in interpreting the brightness and edge detection results. Further refinement of this technique is ongoing.

#### 4.2. Po flood deposit

Several characteristics of the Po flood deposit are worth exploring independent of other river systems. First, to provide a comparison to estimates of the riverine suspended-sediment load during the October 2000 flood (Syvitski and Kettner, 2006), as well as an estimate of deposit mass based on  $^7\text{Be}$  (Palinkas et al., 2005), we have used the digital X-radiographs to estimate the flood deposit mass. We start by calculating the flood deposit volume based on the isopach map (Fig. 7), and then convert to mass using a bulk density. Rather than use a single estimate of the bulk density for the flood deposit, substantial effort was devoted to measuring bulk density based on the December 2000 digital X-radiographs collected at each station. Due to compaction between emplacement and coring we could not apply our techniques to the October 2001 X-radiographs, and therefore could not interpolate over the same domain as the isopach. Instead, we partitioned the deposit into five regions based on rational combinations of deposit thickness and water depth and used the December 2000 results to estimate an average bulk density in each region. Bulk density values (assuming a grain density of  $2.65 \text{ g/cm}^3$ ) ranged from  $1.52 \text{ g/cm}^3$  (0.69 porosity) for thick deposits in shallow water to  $1.25 \text{ g/cm}^3$  (0.86 porosity) for thin deposits in deep water, with an overall (i.e., derived) deposit bulk density of  $1.4 \text{ g/cm}^3$  (0.77 porosity). Using the volume estimate and the bulk density data we arrived at a mass of  $16 \times 10^9 \text{ kg}$  for the Po River flood deposit. Given the many assumptions and uncertainties in calculating the deposit mass (e.g., data coverage, gridding

details) this estimate is consistent with another ( $13 \times 10^9 \text{ kg}$ ) based on  $^7\text{Be}$  (Palinkas et al., 2005). Moreover, we would expect the earlier estimate to be lower, since it appears that the sediment discharged in the early portion of the flood was depleted in  $^7\text{Be}$ , and was therefore not accounted for in the calculations made by Palinkas et al. (2005).

Our flood deposit mass can be compared to the cumulative river suspended sediment load during the fall 2000 flood (1 October to 3 December) made by Syvitski and Kettner (2006) based on model simulations using HYDROTREND (a river discharge simulator). Their results range from a high of  $42 \times 10^9 \text{ kg}$  for the natural river without any trapping in the delta to a low of  $7.5 \times 10^9 \text{ kg}$  for the human impacted river with trapping, and a mean of  $24 \times 10^9 \text{ kg}$  (Syvitski and Kettner, 2006). While the variability in the HYDROTREND calculations ( $\sim 6 \times$ ) reflects the difficulty of predicting the complex nature of rivers, we can perhaps use the flood deposit mass to rule out some of the load scenarios. First, it is unlikely that the deposit mass estimate was too high by a factor of two, thus the low-end load estimate, which is derived from trapping  $\sim 16\%$  of the load in the delta and reducing the resultant load by a further 50%, is probably not correct. Alternatively, the high-end load scenario almost certainly is not accurate in that we know humans have altered extensively the Po River for centuries (e.g., Marchi et al. 1996), and that a non-zero fraction of the load must be trapped in the delta. Using the mean estimate ( $24 \times 10^9 \text{ kg}$ ) implies that roughly two-thirds of the flood sediment load can be accounted for in the deposit. While there are certainly large uncertainties in these calculations, they do suggest that a higher proportion of the flood sediment can be accounted for in the Po flood deposit compared to the Eel flood deposits ( $\sim 25\%$ ) (Wheatcroft et al., 1997; Wheatcroft and Borgeld, 2000). This higher retention in the near field is consistent with the facts that the river sediment was pre-flocculated, resulting in high settling velocities from the surface plume (Fox et al., 2004; Milligan et al., 2006) and wave energy was generally low during emplacement (see below).

Irrespective of the total mass of sediment delivered and found on the Po prodelta slope, we can examine the relative partitioning of sediment adjacent to the different river mouths. Ideally this would have been done for the Pila, Tolle and Gnocca/Goro distributaries, however, the deposit

was fairly continuous alongshore between the Tolle and Gnocca/Goro (Fig. 7) and any separation would have been arbitrary. We therefore took a more conservative approach and simply separated the deposit mass north and south of 44.9°N, the approximate location of the large mussel farm (Fig. 7). Results indicate 43% of the deposit is in the northern subregion (i.e., Pila), whereas the remaining 57% is in the south (i.e., Tolle + Gnocca/Goro). Historical (e.g., Nelson, 1970) and recent (Syvitski et al., 2005) efforts to partition suspended sediment in the various river distributaries indicates up to 80% of the Po River's load exits the Pila mouth. This apparent discrepancy is likely due to two factors. First, the net transport along the delta front is on average to the south (Traykovski et al., 2006), thus almost certainly some fraction of the Pila load was carried south of 44.9°N. Second, it is likely that the secondary distributaries become more active during high discharge events (e.g., Syvitski et al., 2005).

The cross-margin distribution of sediment adjacent to the various distributaries also differs (Fig. 8). Off the Pila (i.e., E line), the flood deposit extends roughly 8 km offshore into water depths of ~29 m, whereas to the south (J and N lines) the deposit's lateral extent and maximal depth both decrease. This pattern is consistent with the cross shelf bathymetry—steep off the Pila, gentle off the Tolle/Goro—and the momentum (and hence seaward extension) of the different plumes. The latter is likely to be high for the Pila, which is the straightest and most frequently dredged of the distributaries, whereas the southern distributaries are smaller and have more sinuous channels. In addition, the complex bathymetry in the vicinity of the Pila mouth, where there is an approximately 90° turn in the coast and bathymetry (Fig. 1), must contribute to lateral spreading of the plume.

#### 4.3. Po–Eel comparison

We focus on a detailed Po–Eel comparison at the expense of other recently documented flood deposits (e.g., Saguenay Fjord: Pelletier et al., 1999; Var: Mulder et al., 2001a, b) for two reasons. First, the general depositional settings of the Eel and Po systems are similar. That is, both rivers discharge into an open, unrestricted continental shelf setting, where waves and coastal currents could potentially affect the distribution and small-scale properties of the resultant flood deposits. In contrast, the

Saguenay Fjord flood deposit documented by Pelletier et al. (1999) was emplaced in a fjord environment where its large-scale distribution was likely set by the geometry of the 3 km × 12 km, steep-walled receiving basin. In addition, coastal currents and waves were unlikely to have affected the deposit during emplacement because the fjord reaches a depth of 100 m with <2 km of the river mouth and there is limited fetch (i.e., waves are minimal). Similarly, the Var flood deposits (Mulder et al., 2001a, b) have been found at 2000 m within a submarine canyon complex, and have been interpreted to be hyperpycnal flow deposits. The second reason for focusing on the Eel–Po comparison is that similar methods were used in documenting these flood deposits, whereas significant differences in sample density (Var) and laboratory analyses (Saguenay Fjord) used by the other studies compromise detailed comparisons. Nevertheless, the Saguenay Fjord and Var fan results, as well as those from other settings (e.g., Drake et al., 1972; Allison et al., 2000), suggest that river floods can form a variety of distinct deposits on continental margins. Determining the minimal set of variables that control the distribution and characteristics of such deposits is a critical future challenge.

There are three important contrasts between the Po and Eel flood deposits: (1) deposit location relative to the river mouth, (2) overall thickness, and (3) stratigraphic complexity. The most salient difference between the Po and Eel River flood deposits is that the former was found immediately adjacent to the distributary mouths in water depths as shallow as 6 m (e.g., Fig. 7). In contrast, the centers of mass of the Eel River flood deposits were displaced northward along-margin by roughly 18 km and were found in water depths of 50–110 m (Wheatcroft and Borgeld, 2000). Related to this difference in flood deposit location is the contrast between the locations of the surface sediment plume and the deposit. In the case of the Eel, helicopter-based CTD/transmissometer sampling of the plume (Geyer et al., 2000; Hill et al., 2000) showed clearly that the sediment plume never extended seaward of approximately 40 m, and therefore did not overlap with the deposit. In contrast, the Po surface sediment plume observed from satellites shows a remarkably close agreement with the footprint of the flood deposit (cf. Syvitski et al., 2005; Milligan et al., 2006).

The location of the Eel and Po flood deposits relative to their respective river mouths is likely

related to differences in their mode of emplacement. In the case of the Eel, the emerging picture is that strong southerly winds during the discharge peaks lead to northward advection of the surface plume (Geyer et al., 2000). High suspended-sediment concentrations in the surface plume result in rapid settling and transport to the bottom boundary layer in shallow water (<40 m) (Hill et al., 2000). Fine-grained sediment does not typically accumulate in shallow water, however, due to high bottom stresses from storm-driven waves. Instead, sediment is maintained in suspension within the wave boundary layer, where it eventually reaches concentrations that allow down-slope, gravity-driven transport as fluid mud flows (e.g., Traykovski et al., 2000; Scully et al., 2003).

In contrast, the distribution of the Po flood deposit matches almost identically the pattern of the surface plume as observed from satellites (Milligan et al., 2006). This correspondence, as well as the close agreement between the mass fraction of flocs in the deposit (Milligan et al., 2006) and the river during a range of flow conditions (Fox et al., 2004), suggests that direct fallout from the surface plume was the dominant mode of sediment delivery to the seabed during the flood. Density-driven transport may also have occurred, however, as implied by the theoretical arguments of Friedrichs and Scully

(2006) and supported by limited indirect evidence. The latter comes from a single site (ED20) off the Pila distributary (Fig. 11). There, X-radiographs reveal a completely structureless, X-ray opaque bed that is roughly 9 cm thick, and grain size analyses show that it *coarsens* upwards (Fig. 11). This grain size pattern is similar to that reported by Mulder et al. (2001b) for the Var River hyperpycnal flood deposits, and is interpreted to reflect an increase in flow capacity as the river discharge peaks. Interestingly, station ED20 is located in the region of maximal slope adjacent to the main distributary (Fig. 1), thus if a hyperpycnal flow did occur during the Po flood it would likely be in that general region (Friedrichs and Scully, 2006).

A second difference between the Eel and the Po flood deposits involves their relative thickness. The maximal thickness observed for the Eel flood deposits was 8 cm, whereas the Po flood deposit was up to 36 cm thick at one site and >20 cm at many other locations (e.g., Fig. 7). These overall thickness differences translate to relatively small horizontal thickness gradients for the Eel (e.g., 8-cm change in 12 km along-shelf), compared to extremely sharp horizontal thickness gradients on the Po (e.g., 10-cm change in 1.1 km along-shelf). Although the Eel gradients are larger in the across-shelf direction, they are still a factor of three less than the

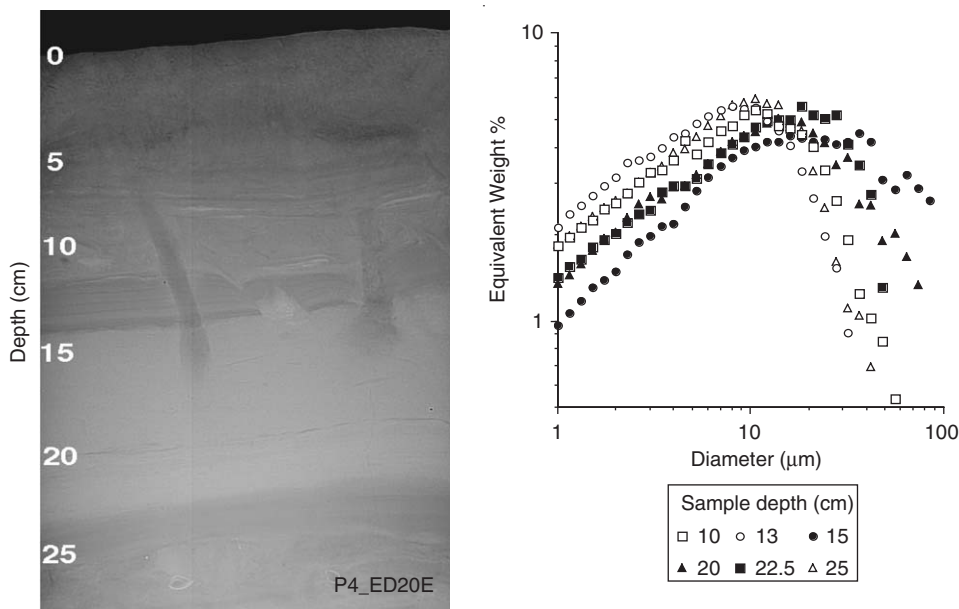


Fig. 11. X-radiograph from station ED20 (October 2001) showing a ~9-cm thick X-ray opaque layer (14–23 cm depth). Grain size analyses at several depths within the core indicate that the X-ray opaque layer coarsens upward and is very poorly sorted.

Po cross-shelf gradients (Fig. 8). Collectively, these differences suggest that the Eel system is much more dispersive than the Po. Reasons for the lower dispersivity of the Po is that the energy levels during emplacement of the Po flood deposit were likely much lower than they were during the Eel floods, which is consistent with the lower wind speeds and hence wave heights in the Adriatic compared to the north Pacific. In addition, the pre-flocculated nature of the Po River sediment (Fox et al., 2004) causes rapid settling adjacent to the river mouths.

Not only was the Po flood deposit much thicker than the Eel, it was also more stratigraphically and texturally complex (Figs. 6 and 9–11). In particular, the Po flood deposit displayed a composite internal geometry with multiple layers that ranged from submillimeter laminations to massive beds, >10 cm thick. A diverse suite of physical sedimentary structures, including ripple cross-laminations and lenticular bedding, as well as dramatic vertical changes in grain size (Figs. 6, 10, 11), suggest significant variations in energy levels during deposition of the flood deposit. In addition, soft-sediment deformation structures and vertical variations in the bulk density suggest differences in the rate of deposition during the flood. This complexity is likely due to the fact that the Po flood deposit was formed over a longer time period, during which conditions within the river (e.g., discharge, Fig. 2) and coastal ocean (e.g., waves) varied. In contrast, the internal stratigraphy of the Eel flood deposits is quite simple (Wheatcroft and Borgeld, 2000), implying that the conditions in the bottom boundary layer during floods is relatively similar and the flood deposits are formed over short time periods.

All of the above differences—the location, overall thickness, stratigraphic complexity, and budgets—can best be explained by differences in the riverine source basin size, which controls the *timing and duration* of sediment delivery to the coastal ocean. The Eel River basin is relatively small ( $\sim 9 \times 10^3 \text{ km}^2$ ), hence floods are short-lived (2–3 days) and sediment is delivered during the storm that delivered the precipitation to the basin (Wheatcroft et al., 1997). Thus, energy levels are elevated over fair-weather conditions, and the range of oceanic conditions (e.g., wave height, current speeds) during the flood is small. In contrast, because the Po River basin is roughly eight times larger than the Eel, flood waves require many days to weeks to travel through the basin (e.g., Fig. 2). This relatively long temporal lag means that the

pulse (or pulses) of elevated suspended sediment that is delivered to the ocean occurs during a range of oceanic conditions (i.e., the storm responsible for the precipitation is long gone), the majority of which are reflective of the fair-weather condition. Sediment is therefore deposited proximal to the river mouths, where it can form thick, but stratigraphically complex deposits.

## 5. Summary

River basin size is emerging as a key factor in determining the location and character of flood deposits in the prodelta region. On the large end of the spectrum (e.g., basin  $> 10^5 \text{ km}^2$ ), for example, the Columbia or Amazon, sediment delivery occurs over seasonal time scales, and the river–ocean system is decoupled. Event-driven sediment delivery is essentially non-existent because the large size of the river basin acts to dampen any precipitation spikes. The character and distribution of sediment on the adjacent continental margin is determined by local oceanographic forcing, sometimes operating during the season of low river discharge (e.g., Columbia, Sternberg, 1986). On the small end of the river spectrum (e.g.,  $< 10^4 \text{ km}^2$ ), for example, the Eel or Waipaoa (Hicks et al., 2000), sediment throughput time is measured in hours to days, and the river–ocean system is strongly coupled (Wheatcroft et al., 1997). That is, virtually all sediment that is delivered to the coastal ocean occurs during episodic, highly energetic events. Thus, flood sediment is widely dispersed, resultant beds are apt to be relatively thin, and the deposit is stratigraphically simple (e.g., Wheatcroft and Borgeld, 2000).

Between the two end members (i.e., basin size  $10^4$ – $10^5 \text{ km}^2$ ), are rivers such as the Po and Rhone (basin size:  $95,500 \text{ km}^2$ , mean discharge:  $\sim 1700 \text{ m}^3/\text{s}$ ; Lique et al., 2004). Although these rivers are small enough to support event-driven floods, they can also act like large rivers. The deciding factor is the location, relative to the river mouth, of the precipitation that creates the flooding. In the case of the October 2000 event on the Po, the precipitation occurred far up in the western reaches of the basin and the flood wave took several days to weeks to travel through the system (e.g., Fig. 2). Thus, sediment was delivered during mostly fair-weather conditions, and was therefore deposited proximal to the river mouth in a thick, stratigraphically complex deposit. In this sense, the Po “acted” more like a larger river. If the precipitation had occurred closer

to the river mouth, then sediment discharge would more likely occur during energetic conditions. Determining the utility of these ideas concerning the role that river-basin size plays in controlling the distribution and character of oceanic flood deposits will require additional studies.

## Acknowledgments

This study could not have been conducted without the support of colleagues at the Istituto di Scienze Marine, Sezione di Geologia Marina di Bologna (CNR), especially Stefano Miserocchi, Fabio Trincardi and Anna Correggiari. Their help, as well as that provided by other participants (A. Boldrin, A. Cattaneo, C. Fritz, C. Nittrouer, A. Ogston and D. Ridente) in the December rapid-response cruise, was critically important. We also thank the responsiveness of the ONR program officer, Jill Karstens (now at AGU), for financial support to mount the event response. Lastly, we benefited greatly from the comments of three anonymous journal reviewers, and although we may not have agreed with all their points, we appreciate their efforts on our behalf. Supported by Office of Naval Research Grant N00014-02-1-0067.

## References

- Allison, M.A., Kineke, G.C., Gordon, E.S., Goñi, M.A., 2000. Development and reworking of a seasonal flood deposit on the inner continental shelf off the Atchafalaya River. *Continental Shelf Research* 20, 2267–2294.
- Andrews, D., Bennett, A., 1981. Measurements of diffusivity near the sediment–water interface with a fine-scale resistivity probe. *Geochimica et Cosmochimica Acta* 45, 2169–2175.
- Boldrin, A., Bortoluzzi, G., Frascari, F., Guerzoni, S., Rabitti, S., 1988. Recent deposits and suspended sediments off the Po della Pila (Po River, main mouth), Italy. *Marine Geology* 79, 159–170.
- Dance, D.R., 1988. Diagnostic radiology with X-rays. In: Webb, S. (Ed.), *The Physics of Medical Imaging*. IOP Publishing, Bristol, pp. 20–73.
- Davis, J.C., 1986. *Statistics and Data Analysis in Geology*, 2nd ed. Wiley, New York.
- Drake, D.E., 1999. Temporal and spatial variability of the sediment grain-size distribution on the Eel shelf: the flood layer of 1995. *Marine Geology* 154, 169–182.
- Drake, D.E., Kolpack, R.L., Fischer, P.J., 1972. Sediment transport on the Santa Barbara–Oxnard shelf, Santa Barbara Channel, California. In: Swift, D.J.P., Duane, D.B., Pilkey, O.H. (Eds.), *Shelf Sediment Transport: Process and Pattern*. Dowden, Hutchinson and Ross, New York, pp. 307–331.
- Fox, J.M., Hill, P.S., Milligan, T.G., Boldrin, A., 2004. Flocculation and sedimentation on the Po River delta. *Marine Geology* 203, 95–107.
- Frey, R.W., Pemberton, S.G., 1990. Bioturbate texture or ichnofabric? *Palaios* 5, 385–386.
- Friedrichs, C.T., Scully, M.E., 2006. Modeling deposition by wave-supported gravity flows on the Po River prodelta: From seasonal floods to prograding clinoforms. *Continental Shelf Research* 26, xxx–xxx (in press).
- Frignani, M., Langone, L., Ravaioli, M., Sorgente, D., Alvisi, F., Albertazzi, S., 2005. Fine sediment mass balance in the western Adriatic continental shelf over a century time scale. *Marine Geology* 222/223, 113–133.
- Geyer, W.R., Hill, P.S., Milligan, T.G., 2000. The structure of the Eel River plume during floods. *Continental Shelf Research* 20, 2067–2094.
- Gomez, B., Mertes, L.A.K., Phillips, J.D., Magilligan, F.J., James, L.A., 1995. Sediment characteristics of an extreme flood: 1993 upper Mississippi River valley. *Geology* 23, 963–966.
- Gonzalez, R.C., Wintz, P., 1987. *Digital Image Processing*, 2nd ed. Addison-Wesley, Reading, MA.
- Hamblin, W.K., 1962. X-ray radiography in the study of structures in homogeneous sediments. *Journal of Sedimentary Petrology* 32, 201–210.
- Hicks, D.M., Gomez, B., Trustrum, N.A., 2000. Erosion thresholds and suspended sediment yields, Waipaoa River basin, New Zealand. *Water Resources Research* 36, 1129–1142.
- Hill, P.S., Milligan, T.G., Geyer, W.R., 2000. Controls on effective settling velocity of suspended sediment in the Eel River flood plume. *Continental Shelf Research* 20, 2095–2112.
- Howard, J.D., 1968. X-ray radiography for examination of burrowing by marine invertebrate organisms. *Sedimentology* 11, 249–258.
- Inman, D.L., Jenkins, S.A., 1999. Climate change and the episodicity of sediment flux of small California rivers. *Journal of Geology* 107, 251–270.
- Jähne, B., 1991. *Digital Image Processing*. Springer, Berlin.
- Kranck, K., Milligan, T.G., 1991. Grain size in oceanography. In: Syvitski, J.P.M. (Ed.), *Theory, Methods and Applications of Particle Size Analysis*. Cambridge University Press, New York, pp. 332–345.
- Krinitzsky, E.L., 1970. *Radiography in the Earth Sciences and Soil Mechanics*. Plenum Press, New York.
- Leithold, E.L., Hope, R.S., 1999. Deposition and modification of a flood layer on the northern California shelf: lessons from and about the fate of terrestrial particulate organic carbon. *Marine Geology* 154, 183–195.
- Liquete, C., Canals, M., Arnau, P., Urgeles, R., Durrieu de Madron, X., 2004. The impact of humans on strata formation along Mediterranean margins. *Oceanography* 17, 70–79.
- Marchi, E., Roth, G., Siccardi, F., 1996. The Po: centuries of river training. *Physics and Chemistry of the Earth* 5/6, 475–478.
- Meade, R.H., 1966. Factors influencing the early stages of compaction of clays and sands—review. *Journal of Sedimentary Petrology* 36, 1085–1101.
- Migeon, S., Weber, O., Faugeres, J.-C., Saint-Paul, J., 1999. SCOPIX: a new X-ray imaging system for core analysis. *Geo-Marine Letters* 18, 251–255.
- Milligan, T.G., Kranck, K., 1991. Electro-resistance particle size analysers. In: Syvitski, J.P.M. (Ed.), *Theory, Methods and*

- Applications of Particle Size Analysis. Cambridge University Press, New York, pp. 109–118.
- Milligan, T.G., Hill, P.S., Law, B.A., 2006. Grain size evolution of the October 2000 Po River flood deposit. *Continental Shelf Research* 26, xxx–xxx (in press).
- Milliman, J.D., Syvitski, J.P.M., 1992. Geomorphic/tectonic control of sediment discharged to the ocean: the importance of small mountainous rivers. *Journal of Geology* 100, 525–544.
- Mulder, T., Syvitski, J.P.M., 1995. Turbidity currents generated at river mouths during exceptional discharges to the world oceans. *Journal of Geology* 103, 285–299.
- Mulder, T., Migeon, S., Savoye, B., Jouanneau, J.-M., 2001a. Twentieth century floods recorded in deep Mediterranean sediments. *Geology* 29, 1011–1014.
- Mulder, T., Migeon, S., Savoye, B., Faugeres, J.-C., 2001b. Inversely graded turbidite sequences in the deep Mediterranean: a record of deposits from flood-generated turbidity currents? *Geo-Marine Letters* 21, 86–93.
- Nelson, B.W., 1970. Hydrography, sediment dispersal, and recent historical development of the Po River delta, Italy. In: Morgan, J.P. (Ed.), *Deltaic Sedimentation: Modern and Ancient*. Society of Economic Paleontologists and Mineralogists Special Publication 15. Tulsa, Oklahoma, pp. 152–184.
- Nittrouer, C.A., Sternberg, R.W., Carpenter, R., Bennett, J.T., 1979. The use of  $^{210}\text{Pb}$  geochronology as a sedimentological tool: application to the Washington continental shelf. *Marine Geology* 31, 297–316.
- Orsi, T.H., Edwards, C.M., Anderson, A.L., 1994. X-ray computed tomography: a nondestructive method for quantitative analysis of sediment cores. *Journal of Sedimentary Research A* 64, 690–693.
- Palinkas, C.M., Nittrouer, C.A., Wheatcroft, R.A., Langone, L., 2005. The use of  $^7\text{Be}$  to identify event and seasonal sedimentation near the Po River delta, Adriatic Sea. *Marine Geology* 222/223, 95–112.
- Pavese, M.P., Banzon, V., Colacino, M., Gregori, G.P., Pasqua, M., 1992. Three historical data series of flood and anomalous climatic events in Italy. In: Bradley, R.S., Jones, P.D. (Eds.), *Climate Since A.D. 1500*. Routledge, New York, pp. 155–170.
- Pelletier, È., Deflandre, B., Nozais, C., Tita, G., Desrosiers, G., Gagné, J.P., Mucci, A., 1999. Crue éclair de juillet 1996 dans la région du Saguenay (Québec). 2. Impacts sur les sédiments et le biote de la baie des Ha! Ha! Et du fjord du Saguenay. *Canadian Journal of Fisheries and Aquatic Science* 56, 2136–2147.
- Ratto, S., Bonetto, F., Comoglio, C., 2003. The October 2000 flooding in Valle d'Aosta (Italy): event description and land planning measures for risk mitigation. *International Journal of River Basin Management* 1, 105–116.
- Regione Emilia-Romagna, 2001. Eutrofizzazione delle acque costiere dell'Emilia-Romagna. Rapporto Annuale 2000, 230pp.
- Restrepo, J.D., Kjerfve, B., 2000. Water discharge and sediment load from the western slopes of the Colombian Andes with a focus on the Rio San Juan. *Journal of Geology* 108, 17–33.
- Russ, J.C., 1995. *The Image Processing Handbook*, 2nd ed. CRC Press, Boca Raton, FL.
- Scully, M.E., Friedrichs, C.T., Wright, L.D., 2003. Numerical modeling results of gravity-driven sediment transport and deposition on an energetic continental shelf: Eel River, Northern California. *Journal of Geophysical Research* 108, 17–17-14.
- Sokal, R.R., Rohlf, F.J., 1981. *Biometry*, 2nd ed. W.H. Freeman and Company, New York.
- Sommerfield, C.K., Nittrouer, C.A., Alexander, C.R., 1999.  $^7\text{Be}$  as a tracer of flood sedimentation on the northern California continental margin. *Continental Shelf Research* 19, 335–361.
- Sternberg, R.W., 1986. Transport and accumulation of river derived sediment on the Washington continental shelf, USA. *Journal of the Geological Society, London* 143, 953–964.
- Syvitski, J.P.M., Kettner, A.J., Correggiari, A., Nelson, B.W., 2005. Distributary channels and their impact on sediment dispersal. *Marine Geology* 222/223, 75–94.
- Syvitski, J.P.M., Kettner, A.J., 2006. On the flux of water and sediment into the northern Adriatic. *Continental Shelf Research* 26, xxx–xxx (in press).
- Traykovski, P., Geyer, W.R., Irish, J.D., Lynch, J.F., 2000. The role of wave-induced density-driven fluid mud flows for cross-shelf transport on the Eel River continental shelf. *Continental Shelf Research* 20, 2113–2140.
- Traykovski, P., Wiberg, P.L., Geyer, W.R., 2006. Observations and modeling of wave-supported sediment gravity flows on the Po prodelta and comparison to prior observations from the Eel shelf. *Continental Shelf Research* 26, xxx–xxx (in press).
- Trincardi, F., Correggiari, A., Roveri, M., 1994. Late Quaternary transgressive erosion and deposition in a modern epicontinental shelf: the Adriatic semiencloded basin. *Geo-Marine Letters* 14, 41–51.
- Vörösmarty, C.J., Fekete, B.M., Meybeck, M., Lammers, R.B., 2000. Global system of rivers: its role in organizing continental land mass and defining land-to-ocean linkages. *Global Biogeochemical Cycles* 14, 599–621.
- Warrick, J.A., Fong, D.A., 2003. Dispersal scaling from the world's rivers. *Geophysical Research Letters* 31, L04301, doi:10.1029/2003GL019114.
- Weisfield, R.L., Hartney, M.A., Street, R.A., Apte, R.B., 1998. New amorphous-silicon image sensor for X-ray diagnostic medical imaging applications. *SPIE Medical Imaging 1998. Physics of Medical Imaging* 3336, 444–452.
- Wheatcroft, R.A., 2000. Oceanic flood sedimentation: a new perspective. *Continental Shelf Research* 20, 2059–2066.
- Wheatcroft, R.A., 2002. In situ measurements of near-surface porosity in shallow-water marine sands. *IEEE Journal of Oceanic Engineering* 27, 561–570.
- Wheatcroft, R.A., 2006. Time-series measurements of macrobenthos abundance and sediment bioturbation intensity on a flood-dominated shelf. *Progress in Oceanography* (in review).
- Wheatcroft, R.A., Borgeld, J.C., 2000. Oceanic flood layers on the northern California margin: large-scale distribution and small-scale physical properties. *Continental Shelf Research* 20, 2163–2190.
- Wheatcroft, R.A., Sommerfield, C.K., Drake, D.E., Borgeld, J.C., Nittrouer, C.A., 1997. Rapid and widespread dispersal of flood sediment on the northern California continental margin. *Geology* 25, 2059–2190.
- Wilson, R., Spann, M., 1988. *Image Segmentation and Uncertainty*. Wiley, New York.